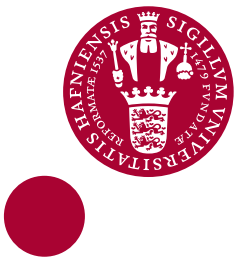

Origin and Dynamics ofSaltwater Intrusion in a Regional Aquifer

Combining 3-D Saltwater Modeling With Geophysical and Geochemical Data

Meyer, Rena; Engesgaard, Peter; Sonnenborg, Torben Obel

Published in:
Water Resources Research

DOI:
10.1029/2018WR023624

Publication date:
2019

Document version
Publisher's PDF, also known as Version of record

Water Resources Research

RESEARCH ARTICLE
10.1029/2018WR023624

Origin and Dynamics of Saltwater Intrusion in a Regional Aquifer: Combining 3-D Saltwater Modeling With Geophysical and Geochemical Data

Rena Meyer[1], **Peter Engesgaard**[1], **and Torben O. Sonnenborg**[2]

[1]Department of Geosciences and Natural Resource Management, University of Copenhagen, Copenhagen, Denmark, [2]Geological Survey of Denmark and Greenland, Copenhagen, Denmark

Key Points:
- Paleo sea level changes were needed to identify origin and dynamics of present saltwater intrusion
- Airborne Electromagnetic data showed potential in constraining parameters and validating model assumptions
- Climate change scenarios show that salinization of deep aquifers relate to nonstationarity, and in shallow ones it is due to sea level rise

Supporting Information:
- Supporting Information S1

Correspondence to:
R. Meyer,
reme@ign.ku.dk

Citation:
Meyer, R., Engesgaard, P., & Sonnenborg, T. O. (2019). Origin and dynamics of saltwater intrusion in a regional aquifer: Combining 3-D saltwater modeling with geophysical and geochemical data. *Water Resources Research*, *55*, 1792–1813. https://doi.org/10.1029/2018WR023624

Received 13 JUL 2018
Accepted 18 JAN 2019
Accepted article online 22 JAN 2019
Published online 1 MAR 2019

Abstract Worldwide, aquifers in low-lying coastal areas are threatened by saltwater occurrence, as a result of small head gradients, high groundwater abstraction rates, and drain management of the landscape, which is likely to intensify with climate change. Numerical models can serve as tools to identify the sources of the salt and thus to increase understanding of the driving mechanisms and important parameters controlling the extent of saltwater intrusions. This way, areas vulnerable to sea level rise can be identified and managed. Challenges include unknown initial salt concentrations, heterogeneous geology, and anthropogenic alterations. In this study, hydrogeological, geophysical, and geochemical data are used to develop a numerical density-dependent groundwater flow and transport model with the objective to understand the history of a saltwater-affected groundwater system and its likely response to historic and future changes. The extent of the simulated saltwater intrusion compares well with Airborne Electromagnetic data that show salt water up to 20 km inland. The results reveal that the salt water originates from a combination of laterally intruding seawater and vertically infiltrating transgression water. Main features controlling the progression of the modern seawater into the coastal aquifers are high permeable, deep Miocene sand aquifers, buried valleys that provide preferential flow paths in combination with extensive Miocene clay layers that delay saltwater intrusion. Anthropogenic activity enhances the saltwater inflow from the ocean and induces transient conditions. Future scenarios show that saltwater progression due to nonstationarity leads to enhanced contamination of the deeper aquifers. Climate change affects primarily the shallow aquifer systems.

1. Introduction

Recent studies have demonstrated the global interest in saltwater intrusion in coastal aquifers (e.g., Post & Abarca, 2009; Werner et al., 2013). According to Carrera et al. (2010), the progression of saltwater intrusion is sensitive to (1) coastal topography and water management, (2) type of inland boundary conditions (Werner & Simmons, 2009), (3) geological heterogeneity of coastal aquifers, (4) initial salt distribution, and (5) relative sea level rise. These aspects were addressed in several studies, as summarized in the following; however, research combining all of them is rare. For example, Werner et al. (2013) disclosed the lack of multidisciplinary approaches integrating different types of observational data and numerical modeling.

Saltwater intrusion vulnerability to coastal topography and inland boundary were topics in studies of Michael et al. (2013), Webb and Howard (2011), and Werner and Simmons (2009). In coastal areas, where the water table is close to the ground surface, either because of low topography and/or anthropogenic activities such as land reclamation associated with construction of dikes and drains that keep the water table artificially at a constant low level, sea level rise will enhance saltwater intrusion. Werner and Simmons (2009) found on an analytical basis that head-controlled systems, where the groundwater table is fixed, for example, by drains, are particularly affected by sea level rise. Based on these findings Webb and Howard (2011) presented a numerical study that identified the driving mechanisms of saltwater migration for such head-controlled systems. The factors controlling the toe position of the saltwater wedge were the hydraulic conductivity, recharge, and porosity, while storage parameters were less important. Chang et al. (2011) found that in confined aquifers, near steady state, with constant freshwater fluxes, a sea level rise would lift the hydraulic head and hence mitigate the saltwater intrusion. In unconfined aquifers, this lifting was less effective. However, investigations by Michael et al. (2013) showed that in topography-limited systems, where the

groundwater level is close to the surface, and would intersect it in case of water table rise, sea level rise would mainly result in enhanced surface runoff and therefore limited rise in groundwater levels. Thus, the lifting effect would no longer counteract the progression of the saltwater intrusion. The global importance of these findings becomes clear as Michael et al. (2013) classified up to about 70% of the world coastlines as topography limited. Coastal areas, where drains control the groundwater level, behave similar to topography-limited systems. Large drained coastal systems that are heavily effected by saltwater intrusions have been extensively studied in the Dutch Polder areas (e.g., De Louw et al., 2011; Faneca Sànchez et al., 2012; Oude Essink, 2001; Oude Essink et al., 2010; Pauw et al., 2012).

The importance of the geological architecture and hydrogeological properties of coastal aquifers in controlling the occurrence and progression of saltwater intrusions was pointed out, for example, by Carrera et al. (2010) and Michael et al. (2013). Several modeling studies investigated this aspect using synthetic geological data (Mulligan et al., 2007; Simmons et al., 2001) or for specific locations (e.g., Nishikawa et al., 2009). Nevertheless, the geological complexity was often simplified, especially for regional-scale studies, and only the dominant units and structures were considered (Abarca, 2006). Geological features such as buried valleys (Jørgensen & Sandersen, 2006; Kehew et al., 2012; Piotrowski, 1994), however, may provide preferential flow paths for salt water (Mulligan et al., 2007). A detailed description of the coastal geology is therefore crucial for the understanding of exchange of salt water between sea and aquifers (Jørgensen et al., 2012; Kaleris et al., 2002). Although considerable research has been devoted to understanding the role of geological heterogeneity on saltwater intrusion using two-dimensional models, little attention has been paid to representing complex geological structures in large-scale three-dimensional density-dependent flow and solute transport models and how such structures affect saltwater intrusion.

Whether saltwater intrusion modeling is carried out to study and understand current saltwater intrusions or to simulate their progression in the future due to climate change, assigning the initial salt concentration is crucial (e.g., Hughes et al., 2009). The initial salt distribution is associated with high uncertainties. A common way is to interpolate salt concentrations between observation points (boreholes) sometimes complemented by geophysical data (e.g., Pauw et al., 2012) and use these as initial concentrations. Airborne electromagnetic data have been an efficient way to capture spatial variability in salt concentrations and provided input for saltwater intrusion simulations (Faneca Sànchez et al., 2012; Siemon et al., 2009; Sulzbacher et al., 2012). Subsequently, these models were used to quantify, for example, the effects of climate change on the progression of saltwater intrusion (e.g., Faneca Sànchez et al., 2012; Sulzbacher et al., 2012). Assigning initial salt concentrations in such a way would require steady state of the system. This assumption is often not valid for all locations, and because density-affected groundwater systems react slowly to changing conditions, it can take several hundreds to thousands of years to reach steady state (Webb & Howard, 2011). This is especially an issue in systems where confining beds are present and aquifers are heterogeneous (Hughes et al., 2009). Delsman et al. (2014) simulated the impacts of changing conditions (sea level and land use) during the Holocene on saltwater intrusion in a 2-D transect at the Dutch coastline. Both Hughes et al. (2009) and Delsman et al. (2014) emphasize the limits of applying present-day conditions assuming steady state to derive initial solute concentrations for transport modeling in hydrogeologically complex systems that have undergone significant changes in boundary conditions during the last thousands of years. Past and future conditions (e.g., sea level, water management) were decisive in accurately predicting the evolution of saltwater intrusion in coastal aquifers.

To the authors knowledge the combination of using a realistic, fully three-dimensional, geological model, different types of data on saltwater intrusion, and numerical modeling considering historical and future changes, has not been presented before.

The overall objective of this study is therefore to identify the driving mechanisms that formed a regional saltwater intrusion in a geologically highly complex low-lying coastal environment that has undergone changes in hydraulic conditions as a result of glacial activity, sea level rise during the Holocene and more recent human activities. Jørgensen et al. (2012) observed an extensive saline groundwater body reaching up to ≈20 km inland, using airborne electromagnetic investigation (AEM), in the border region between Denmark and Germany adjacent to the Wadden Sea. The primary objectives of this study are to address the hypothesis by Jørgensen et al. (2012) about (i) the origin of the salt water, (ii) its dynamics, (iii) the role of the geological structure on salinity, and (iv) impacts of future sea level rise. Our secondary objectives include the technicalities to address these questions by the combined results of a density-driven flow and transport

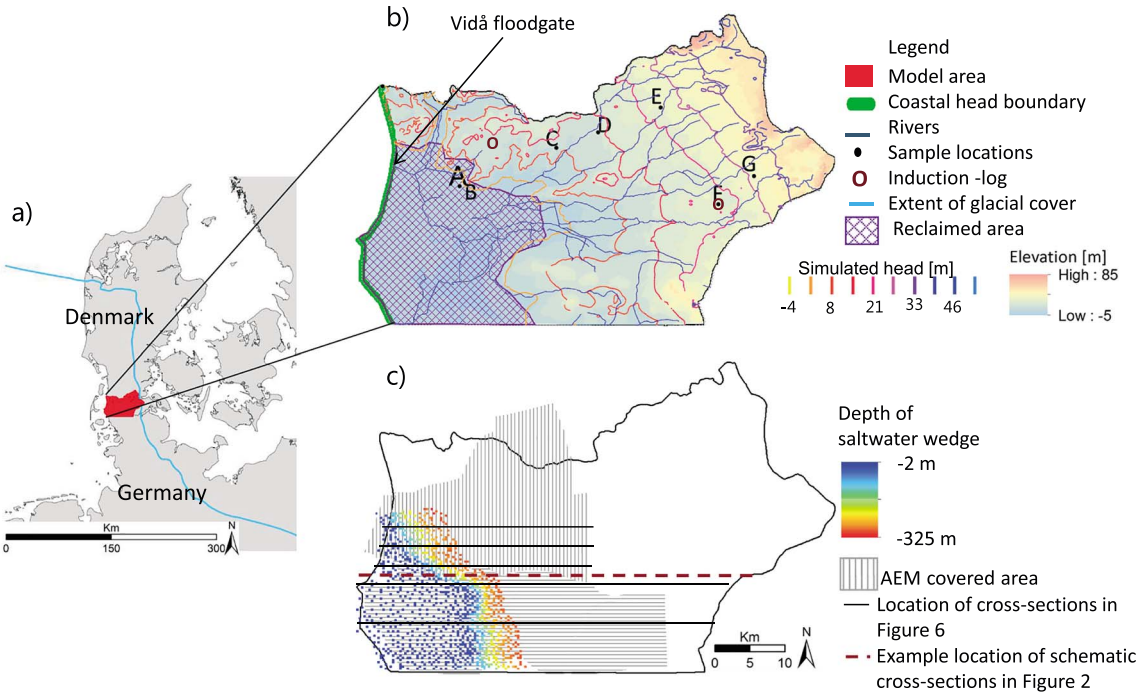

Figure 1. (a) Overview map with location of the investigation area and the maximum extent of the glacial cover during the Weichselian glaciation (blue line). (b) Topography, boundary conditions, simulated head contours as of Meyer et al. (2018a), sampling locations (A–F), locations of two induction logs (Jørgensen et al., 2012; GERDA, http://www.gerda.dk) referred to in the discussion, reclaimed area (formerly flooded, nowadays protected by a dike and heavily drained). (c) Observations: area covered by AEM (gray lines), interpreted depth of saltwater intrusion and locations of cross sections presented in Figures 2 and 6.

model (SEAWAT) against AEM and geochemical data (obtained as a part of this study). The saltwater transgression/regression was simulated in three phases during the last 4200 years. To ascertain the reliability of the model, scenario runs investigated the sensitivity of the salinity pattern to boundary conditions and parameters. Based on the most reliable scenario, the impacts of structural features on density-driven flow and on the formation of the saltwater intrusion during the Holocene are explained. Finally, the response of the saltwater intrusion to climate change (sea level rise, increase in recharge) was quantified with the aim to distinguish between climate change impacts and effects caused by nonstationarity imposed by changing conditions in the past.

2. Study Area

The investigation area covers ≈1,300 km^2 at the Danish-German border adjacent to the Wadden Sea (Figure 1). The western part is a low-lying coastal area with elevations close to, partly below, sea level, while in the east the Jutland ridge reaches elevations up to 85 m. Large areas at the coast (≈300 km^2) were reclaimed from the Wadden Sea during the last couple of centuries. Several dikes and a dense network of drains, keeping the groundwater table constant (in some parts below sea level) made the land arable. Today, the area is mainly used for pasture and some parts are protected as nature reserves. The climate is temperate-maritime with a main wind direction from north to west. The precipitation increases from 900 mm/a at the North Sea to 1,100 mm/a toward the Jutland ridge (Rasmussen et al., 2012).

2.1. Geological and Hydrogeological Evolution

Three main sedimentary facies, spanning from Miocene through Holocene deposits, form the groundwater system in the upper 500 m in the study area (Figure 2). A succession of interlayered Miocene clays and sands, deposited in a deltaic environment, lie on top of the impermeable Palaeogene clay that forms the bottom of the investigated aquifer system. To the west, a thick, mostly homogeneous, layer of upper Miocene marine clay (the Maade formation) forms a low-permeability barrier to the overlying Quaternary sediments. The Pleistocene sediments consist of a glaciotectonic complex of meltwater sand, silt, and glacial till and originated mostly from the Saalian glaciation that covered the whole area. Buried valleys, of Elsterian and

Saalian origin, are abundant in the area and locally cut through the Miocene marine clay (Maade). The Saalian glaciation also left behind a morainic landscape with small hills. In the following Eemian interglacial, large parts of the area were covered by a shallow sea. During the Weichselian, the Scandinavian Ice Sheet (SIS) stored large amounts of water and covered a large part of Northern Europe and as a result, the sea level dropped to ≈120 m below today's level. At this time, the area formed a glacial outwash plain in the direct foreland of a few-hundred-meter-thick ice sheet (Figure 1a; Stroeven et al., 2016). The additional pressure of the ice pack likely affected the hydraulic conditions in the aquifers below the glacier and in the foreland. Likewise, the elevated potentiometric surface in the vicinity of the glacier might have amplified the hydraulic pressure, forming a high hydraulic gradient from the glacier interior toward its margin (Piotrowski, 2007). As a result, the groundwater flow was enhanced in the glacier bed toward and beyond the ice margin. Jørgensen et al. (2012) hypothesized that the Eemian marine salt water might have been flushed out of the subglacial and periglacial aquifers and, hence, the aquifers would contain only fresh water at the end of the Weichselian.

With the thawing of the SIS the hydraulic pressure decreased and at the same time the sea level rose relatively rapidly (Behre, 2007). The shoreline migrated eastward and reached a position close to the present coastline ≈4000 years ago, and salt water started to intrude into the coastal aquifers. The maximum (post-Weichselian) inland inundation extended approximately to the area that is drained today (Figure 1) and lasted until land reclamation started. The first land reclamations started in the sixteenth century, but the area has been permanently protected from flooding only since the highest dikes were constructed in the nineteenth century. Today, a dense network of drains keeps the groundwater table constant, in large parts below the sea level. The water is pumped out from the drains at several locations and into the Vidå river that flows into the North Sea. A floodgate keeps the ocean water outside during high tide (Figure 1). Meyer et al. (2018a) showed that land management changes (artificially low heads in the marsh area due to drainage) and geological features, such as extensive clay layers and buried valleys, are the controlling mechanisms of the regional groundwater flow system (Figure 2). Groundwater flow occurs in the shallow Pleistocene and the deep Miocene aquifer systems, which are separated by the thick Miocene marine clay (Maade), occurring extensively in the west and patchier toward the east. Locally, incised valleys cut through the Maade and allow groundwater exchange between the two aquifer systems. The landward directed head gradient, induced by the drainage network, works as a regional sink and enhances saltwater intrusion from the North Sea.

3. Observations and Methods

3.1. AEM Data

Time domain AEM data were available from several surveys (Sørensen & Auken, 2004) at the German-Danish border between 2004 and 2013 and are stored in the Danish geophysical database (GERDA, http://www.gerda.dk). The surveys cover almost half of the investigation area (Figure 1c) to a depth of ≈200 m with decreasing resolution with depth (Jørgensen et al., 2012). The AEM method is based on electrical properties of the subsurface material. These properties depend on a combination of rock properties and the mineral content in the pore water (saltwater, for example, will decrease the resistivity). Hence, the method is suitable to detect salt water and has been applied in a few saltwater intrusion studies (e.g., Faneca Sànchez et al., 2012; Jørgensen et al., 2012; Sulzbacher et al., 2012). Lithological and chemical borehole data available from the Jupiter database (GEUS, http://www.geus.dk/UK/data,) were used together with the AEM data to delineate the freshwater/saltwater interface in the investigation area (Figure 1c). The transition to salt water is defined by a threshold resistivity of 14 Ωm, which corresponds to the lower limit of formation resistivity to meet EU drinking water standards (Hinsby et al., 2008; Jørgensen et al., 2012).

3.2. Hydrological and Hydrogeochemical Data

In total 1,067 groundwater head measurements were extracted from JUPITER, the Danish national database for geological and hydrological data (GEUS, http://www.geus.dk/UK/data,) and 14 were available within the German part of the area. Distributed net recharge was derived from the national water resources model of Denmark (Henriksen et al., 2003) and stream discharge measurements at three locations for the years 2000–2010 were available (for more details on hydrological data, see ; Meyer et al., 2018a). Groundwater samples from 22 screens at seven locations were collected during a field campaign in February 2015 (well locations A–G, Figure 1c). The samples were analyzed for major ions in the analytical laboratory at GEUS in Copenhagen, Denmark. Of these, 18 were also analyzed for $\delta^{13}C_{‰VPBD}$ and ^{14}C at

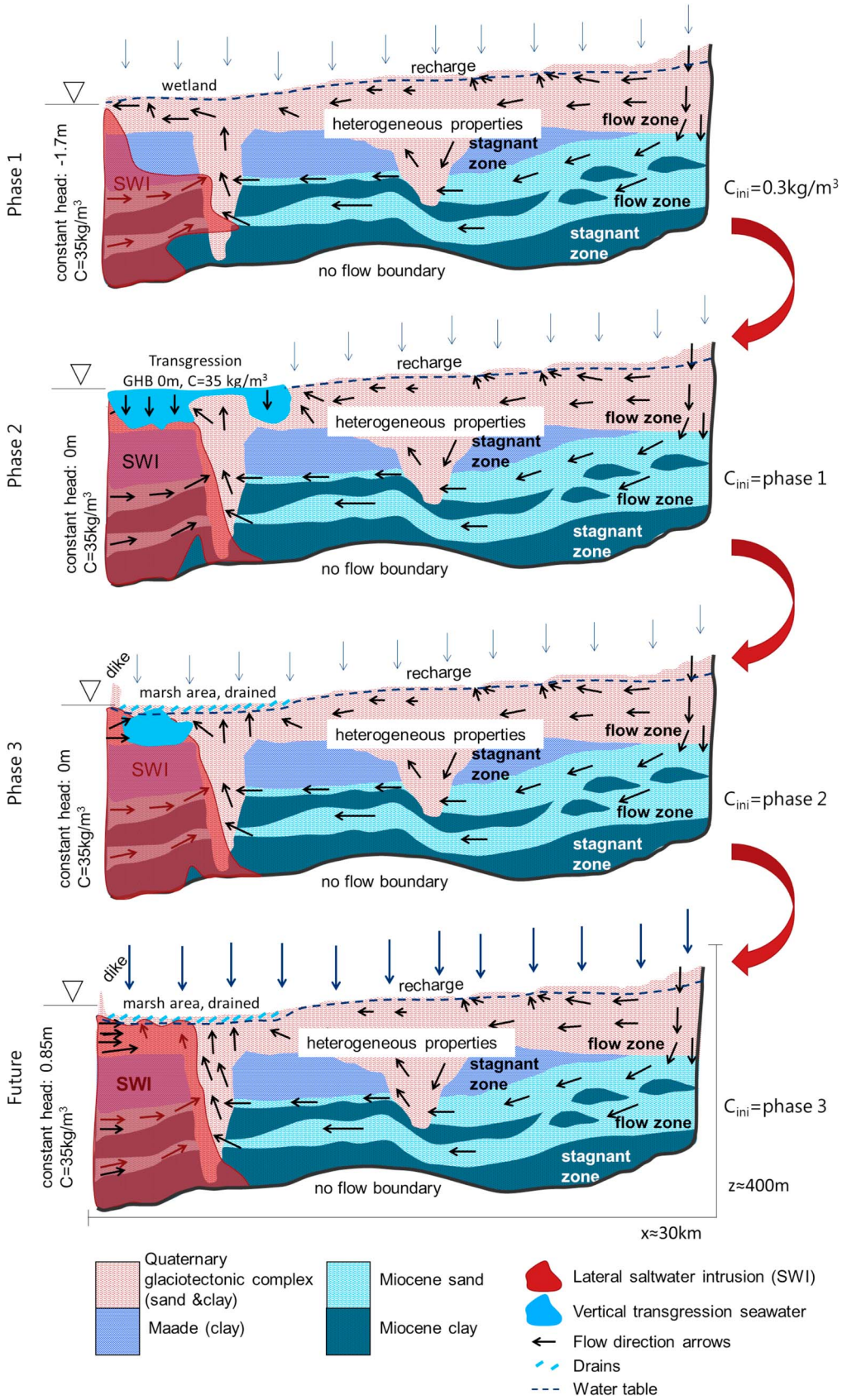

Figure 2. Scheme of boundary conditions and simplified flow fields for the different simulated phases.

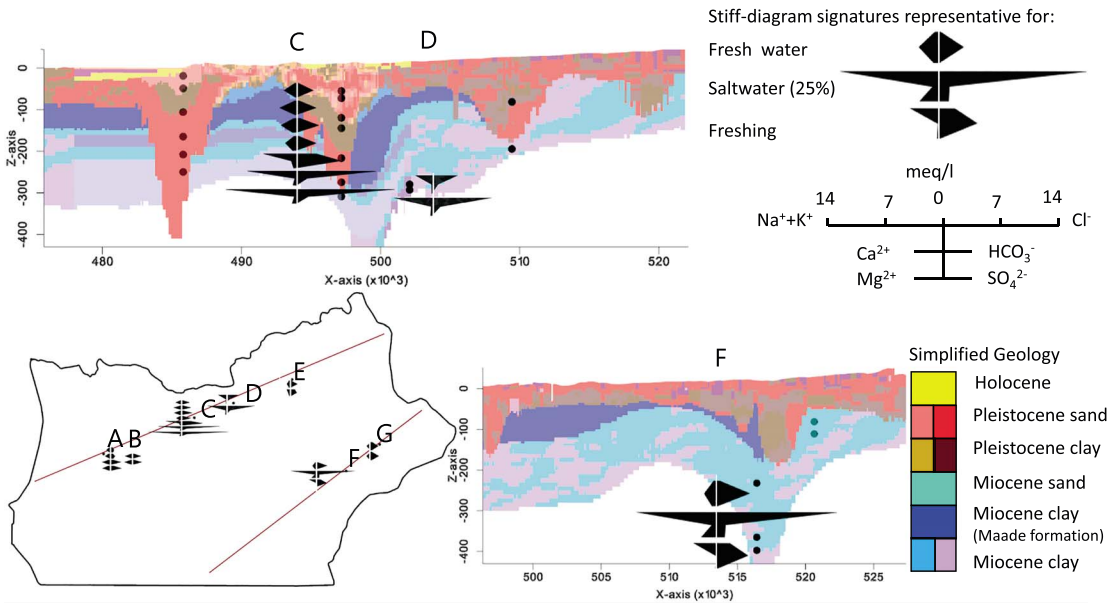

Figure 3. Stiff diagrams in depth compared to geology at locations where salt water patterns are observed. The black dots refer to the exact sample location for which stiff diagrams are shown. Stiff diagrams at the other sampling locations are dominated by freshwater pattern (compare Table 1) and are not added to this Figure for a clear visualization. Simplified description of geology, vertical exaggeration = 30.

the AGH University of Science and Technology in Kraków and the Poznań Radiocarbon Laboratory, Poland (details on radiocarbon dating and the correction terms that had been applied to derive groundwater ages can be found in Meyer et al., 2018b).

3.3. Groundwater State of Intrusion/Refreshing Based on Ion Exchange Processes

The ion composition of groundwater in coastal environments can be used to identify whether the system is in steady state (Appelo & Postma, 2005). In coastal areas, seawater of the NaCl type and fresh water of the $CaHCO_3$ type mixes. The direction of cation exchange can be used to identify different processes. Ca^{2+} dominates the freshwater exchanger. In case of intruding seawater, Ca^{2+} will be released by the exchanger while Na^+ is taken up according to the cation exchange equation (Appelo & Postma, 2005; Stuyfzand, 2008):

$$2Na^+ + CaExch \Longleftrightarrow Ca^{2+} + 2NaExch \quad (1)$$

The water type changes from NaCl to CaCl. In case of refreshing, when fresh water intrudes into salty water, the reverse exchange happens; Na^+ will be exchanged by Ca^{2+} and released. Hereby, the water type changes from $CaHCO_3$ to $NaHCO_3$ (Appelo & Postma, 2005). Information about the water type can give an indication whether intrusion or refreshing is going on. Stiff diagrams are shown in Figure 3 at the sampling locations A–G at different depths. The base exchange index (BEX; Stuyfzand, 2008; Table 1) can additionally be used to identify the direction of the exchange process. For dolomite free conditions apply:

$$BEX = Na^+ + K^+ + Mg^{2+} - 1.0716Cl^-(meq/L) \quad (2)$$

A BEX around zero indicates fresh water, while a negative BEX points toward saltwater intrusion and a positive BEX to refreshing. The significant threshold of the BEX is found as $\pm(0.5 + 0.02\ Cl^-)$ (Stuyfzand, 2008).

3.4. Numerical Model

The model setup and parameter estimates of a calibrated flow and advective transport model using MODFLOW and MODPATH (Meyer et al., 2018a, 2018b) formed the base for simulating saltwater intrusion with SEAWAT. A short summary of the relevant information is provided in the following. The horizontal grid discretization was 200 m × 200 m in the west and 400 m × 200 m in the east, while the vertical discretization was 5 m above 150 m below sea level and 10 m below. No flow boundaries were assigned at the water divide in the

Table 1
Model Phases

Model phase	Time (years BP)	Sea level, boundary conditions	Characteristics
Premodel	≈12000–4200	Retreat of glacial cover, sea level slowly rises, but sea is far away from modern coastline	Aquifer is supposed to be salt free as a result of flushing due to enhanced hydrostatic pressure during glaciation.
1	4200–2200	Sea level rise after Weichselian to −1.7 m asl	Initiation of saltwater intrusion.
2	2200–200	Transgression, sea level at 0 m, marsh area flooded	Salt accumulating in shallow aquifer below flooded area.
3	200–0	Dike was built, land reclamation, modern coastline, sea level 0 m	Refreshing of the upper aquifer.

east, along flow lines in the north and south, and at the bottom of the model defined at the border to Palaeogene clay. Distributed net recharge was available from the Danish national water resource model (Henriksen et al., 2003). In contrast to the previous studies (Meyer et al., 2018a, 2018b) no groundwater abstraction was implemented since abstraction has not taken place in most of the historical periods considered here. Rivers and drains were implemented as head-dependent flux boundaries with estimated conductances of 21.3 $(m^2/d)/m$ and 0.45 $(m^2/d)/m^2$, respectively. Forty-six hydrogeological units were defined based on a heterogeneous voxel geological model (Meyer et al., 2018a). Unit-based horizontal hydraulic conductivity (Kh), vertical hydraulic anisotropy ratio, Kh/Kv, for sand and clay, together with river and drain conductances were estimated using regularized inverse modeling with PEST (Doherty, 2016) based on hydraulic head and average river flow data (Meyer et al., 2018a). Effective porosities (Φ) were estimated for seven units based on ^{14}C age observations (Meyer et al., 2018b). Estimates for Pleistocene sand units of hydraulic conductivities and effective porosities were Kh $\in$ [1; 83 m/d] and $\Phi \in$ [0.13; 0.26], respectively; for Pleistocene clay units Kh $\in$ [0.028; 0.19 m/d] and $\Phi \in$ [0.048; 0.085]; for the Maade formation units Kh $\in$ [0.008; 0.016 m/d] and Φ=0.049; for Miocene sand units Kh $\in$ [16; 46 m/d] and Φ=0.45; and for the Lower Miocene clay units Kh $\in$ [0.14; 0.23 m/d] and $\Phi = 0.1$. A list with all hydrogeological units and the corresponding hydraulic conductivities is presented in the supporting information S1. Vertical hydraulic anisotropy factors (Kh/Kv) were estimated to 25 for sand and to 85 for clay units (Meyer et al., 2018a). Relatively high anisotropy ratios are not uncommon in environments similar to those investigated here (Karan et al., 2014; Sonnenborg et al., 2016; Winter, 1978).

The evolution of the saltwater intrusion throughout the Holocene was simulated with SEAWAT 4 (Langevin et al., 2007), the density-driven flow and transport model of the MODFLOW 2000 family. The simulations were carried out using the finite difference solution scheme with upstream weighting, where flow and transport were explicitly coupled. A phase-wise simulation approach was chosen to satisfy changes in sea level and land use. Hereby, the results from each phase, head and TDS (Total Dissolved Solids) concentrations, served as initial conditions for the next phase. Simplified sea level changes based on Behre (2007) were implemented as a changing boundary condition at the west coast. The different simulation phases and the corresponding boundary conditions are illustrated in Figure 2 and Table 1. Several scenarios were used to investigate the sensitivity of the saltwater intrusion pattern to choices of model boundary conditions and parameters and to identify the most likely scenario that best matches observations of modern saline groundwater body. Similar to Delsman et al. (2014), four mobile species were applied representing “ocean” water (intruding horizontally from the ocean boundary); “transgression” (salt water infiltrating vertically from the flooded area); “local refreshing” (meteoric fresh water infiltrating vertically in the marsh area), and “total refreshing” (meteoric fresh water infiltrating vertically in the total area).

3.4.1. Sensitivity Simulations

3.4.1.1. Base Simulation A

In the base simulation A estimated values for all parameters from Meyer et al. (2018a, 2018b) were used. The simulation started 4200 years before present, where the sea level was close to the present (Behre, 2007). Recharge was constant and equal to modern values during all phases (see below). The geology is represented

in a voxel model that resolves heterogeneity on local scale, and hence, physical dispersion was neglected while diffusion was taken into account with a diffusion coefficient of 8.64×10^{-5} m^2/day as it is a main mechanism of transporting salt from high permeable media into low permeable strata. In principle, the assumption is that, as a result of the higher hydraulic pressure imposed by the SIS, all residual salt water would have been flushed out from the system as hypothesized by Jørgensen et al. (2012). Due to numerical issues, and to avoid negative concentrations, an initial salt concentration of 0.3 kg/m^3 was applied in phase 1 (Figure 2, top) that lasted for a period of 2000 years. A constant head of −1.7 m and a constant salt concentration of 35 kg/m^3 were assigned at the coastal boundary in the west. The reclaimed area was likely not drained to the same extent as presently. However, the land surface elevation in that area is very low, at locations significantly below the present sea level. Hence, the water table, even with a lower sea level, might have been close to the surface and excess water might have been captured by many small streams, resulting in a wetland-type environment. To capture the natural drainage of excess water of such a system, drains located close to the surface (0.1 m below) with a high conductance of 100m^2/d/m^2 were implemented.

In phase 2 (Figure 2, second from top) a transgression with an inundation was simulated for 2000 years. Initial conditions for head and salt concentration were the final results from the end of phase 1. The constant head boundary at the coast was set to 0 m. All cells with an elevation below 1.7 m, corresponding to mean high sea water, were assigned a general head boundary of 0 m with a conductance of 4×10^7 m^2/day and a constant salt concentration of 35 kg/m^3, representing flooding of the area. All wetland drains and recharge in the flooded marsh area were deactivated.

Phase 3 (Figure 2, second from bottom) simulates conditions imposed after the dike construction about 200 years ago, which include heavy drainage below sea level and refreshing of the former flooded area. Here the general head boundary and corresponding constant concentration were removed and modern recharge rates reestablished. Drains were reintroduced to specific levels with conductances estimated by Meyer et al. (2018a).

3.4.1.2. Simulation B: Upper-Parameter Uncertainty Limits

All boundary conditions are the same as in scenario A. The interaction between the marsh area and the ocean in the constant-density model of Meyer et al. (2018a) was found to be sensitive to parameter uncertainty with a 3 times higher inflow through the ocean boundary into the marsh using upper-parameter uncertainty limits (Meyer et al., 2018a). In simulation B the upper uncertainty limits for horizontal and vertical hydraulic conductivities of the 18 identifiable parameters as described by Meyer et al. (2018a) are applied. Hence, a significant change in the extent of the saltwater intrusion compared to scenario A is expected. These upper uncertainty limits are less than half a magnitude higher (a factor of 5) for 13 parameters. The other five parameters change by factors between 5 and 12. Except one parameter, all upper uncertainty limits lie in an expected range for the hydrofacies. The Miocene clay was assigned an unexpected high hydraulic conductivity of 2.05 m/day, which would correspond more to a fine sand.

3.4.1.3. Simulation C: 50% Recharge

In simulation C the groundwater recharge rate during phases 1 and 2 are set to 50% of the modern recharge rate, as a recent study (Karlsson et al., 2014) indicates that historical recharge could have been significantly lower. All other settings are the same as in the base scenario A.

3.4.1.4. Simulation D: With Dispersion

In simulation D the longitudinal, horizontal transversal and vertical transversal dispersivities were set to 50, 5, and 0.5 m, respectively, which are appropriate values for a regional-scale model according to Gelhar et al. (1992). All other settings are as in the base scenario A.

3.4.1.5. Simulation E: Higher Sea Level

To investigate the sensitivity of the salt water distribution to the coastal boundary, the sea level in each phase of simulation E is set to 2.7 m higher than in the base scenario (corresponding to 1 m above modern mean high sea level) while all other settings stay the same.

3.4.2. Future Climate Change Simulation

The impacts of anthropogenic climate changes on the progression of the saltwater intrusion are simulated with initial conditions based on results of phase 3 of scenario B (Figure 2, bottom). An increase in recharge of 10% was applied (corresponding in magnitude to estimates by Van Roosmalen et al., 2009). A relative increase in sea level of 0.85 m based on a combination of sea level rise (Church et al., 2013) and isostatic downwarping of ≈0.25 mm/a (Hansen et al., 2012) over 200 years represents a moderate change compared to scenarios in IPCC5 (Church et al., 2013). These changes in boundary conditions, assuming a linear increase

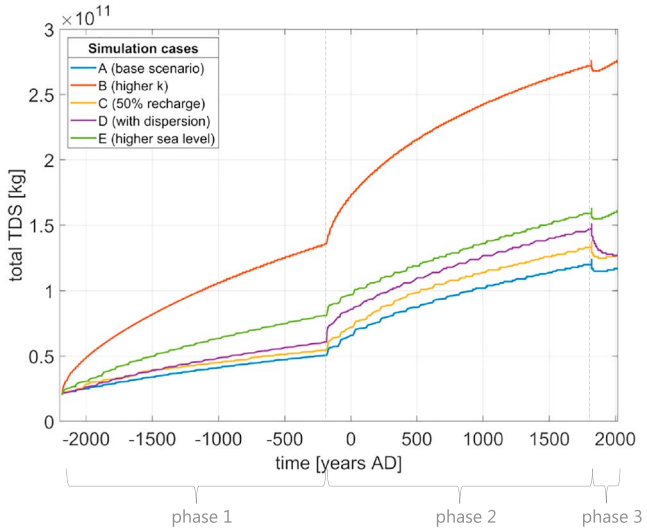

Figure 4. Total amount of total dissolved solid (TDS) over time for the different simulation cases. Sensitivity analysis of parameters and boundary conditions of cases A–E.

in recharge and sea level, were imposed in four steps, each 50 years long. This simulation is referred to as "future -CC" in the following. Moreover, a 200-year simulation under present boundary conditions (referred to "future-steady") enables to distinguish between the effect of climate change and nonstationarity.

4. Results

4.1. Hydrogeochemical Results

Stiff diagrams (Figure 3) show a high concentration of saltwater (NaCl type) at well locations C–F, while at well locations A, B, and G (Figure 3) all samples contain freshwater of $CaHCO_3$ composition. The multiscreen well C, located in a buried valley, has seven screens. The four shallow screens, C7, C6, C5, and C4, contain fresh water (Figure 3, Table 2). At the deeper screen C3 the water is of a $NaHCO_3$ type and both stiff diagrams and the positive BEX index indicate refreshing. The two deepest samples C2 and C1 contain water of NaCl composition with the tendency of intrusion (screen C2; negative BEX) and refreshing (screen C1; positive BEX). The three screens C1–C3 are located deep in the buried valley, confined by an overlying clay layer (Figure 3). Particle back-tracking (Meyer et al., 2018b) identified the recharge locations for these three wells to be far to the east, at the Jutland ridge. Particle paths to C1 and C2 go through Miocene sand and clay deposits only; particles to C3 travel horizontally in the last part through Pleistocene sediments along a buried valley in a regional depression structure. Samples from screens D1 and D2, both located deep in a Miocene sand unit, show salt water of NaCl type and the BEX close to zero indicates that the water is in a chemical equilibrium (Figure 3, Table 2). At well location F, the shallow screen F3 contains fresh water of $CaHCO_3$ type, while the samples from screen F2 show saltwater of NaCl type and from F1 water of $NaHCO_3$ type; in both samples the positive BEX indicates refreshing. All samples indicating saltwater intrusion are found in well screens that are located at depths below 250 m, hence too deep to compare to AEM data (see below). The hydrogeochemistry results show that the deeper aquifer complex is not in a chemical equilibrium.

4.2. Density-Driven Flow Model

4.2.1. Sensitivity Analysis

The sensitivity of the total amount of TDS present in the system during the different model phases to changes in parameters and boundary conditions as defined in simulation scenarios B–E compared to the base scenario A are shown in Figure 4. The base scenario A has the lowest total TDS load compared to the other scenarios. The TDS load increases with initializing saltwater intrusion in phase 1 and during the transgression in phase 2, while in phase 3 refreshing reduces the salt load at first before it increases as a result of drainage. Jumps in the TDS mass result from the step-wise changes in boundary conditions. A reduction in groundwater recharge by 50% between phases 1 and 2 (scenario C) results in an average increase in the total amount of TDS in the system of 10% (in average over all phases). Including physical dispersion (scenario D) increases the TDS amount on average by 18%. Increasing the sea level by 2.7 m (scenario E) in each phase increases the TDS on average by 40%. However, for cases A and C–E, no clear change in the spatial extent of the saltwater intrusion could be recognized on the regional scale (hence not shown for brevity). The application of the upper parameter uncertainty limits (scenario B) yields a much higher increase in TDS present in the system and a significant further intrusion of salt water. Hence, base scenario A and scenario B will be compared to AEM data and the AEM-derived saltwater/freshwater interface to explore the underlying intrusion mechanisms and origin of salt water.

4.2.2. Model Validation—Comparison with AEM

Figure 5 shows horizontal slices of AEM data at different depths (the color scale was adjusted to low resistivities with resistivities above 23 Ωm shown in blue) together with slices through the geological model, and the saltwater intrusion as simulated in scenarios A and B (at the end of phase 3), respectively. Likewise, the AEM data, geology, and simulation results are shown at several vertical cross sections in Figure 6. The interpreted saltwater/freshwater interface, representing the limit for EU drinking water standard of 250 mg/L chloride, is compared to the simulated extent of a TDS concentration of 0.5 kg/m^3, which corresponds approximately

Table 2
Sample Locations (Ordered From Deep to Shallow Filter at Each Location); Aquifer Geology and Structure (BV = buried valley); BEX index; measured ^{14}C, and in situ EC

Well	DGU no.	Filter depth (m b.s.)	Aquifer geology (structure)	BEX (interpretation: intrusion/refresh)	BEX significance	Measured ^{14}C (pMC)	In situ EC (μS/cm)
A1	166.761-1	246–252	Quaternary (BV)	1.27	0.54	46.44	855
A2	166.761-2	204–210	Quaternary (BV)	1.00	0.53	49.95	786
A3	166.761-3	38–40	Quaternary sand	0.85	0.53	—	334.5
A4	166.761-4	18–20	Quaternary sand	0.64	0.52	—	537.5
B1	166.762-1	160–166	Quaternary (BV)	0.39	0.52	49.84	676
B2	166.762-2	102–108	Quaternary (BV)	0.37	0.51	51.9	609
C1	167.1545-1	306–312	Quaternary (BV)	22.81 (refresh)	3.36	0.48	17115
C2	167.1545-2	273–276	Quaternary (BV)	-3.18 (intrusion)	2.82	1.03	13590
C3	167.1545-3	215–218	Quaternary (BV)	12.86 (refresh)	0.64	0.16	2260
C4	167.1545-4	142–149	Quaternary (BV)	1.64	0.51	33.84	683
C5	167.1545-5	116–123	Quaternary (BV)	1.14	0.52	43.18	817
C6	167.1545-6	70–76	Quaternary sand	0.19	0.52	—	740
C7	167.1545-7	53–56	Quaternary sand	0.24	0.51	—	642.5
D1	159.1335-1	290–295	Miocene	−0.08	1.40	1.8	5495
D2	159.1335-2	277–282	Miocene	0.14	0.88	1.35	2600
E1	159.1444-1	194–200	Buried valley	0.88	0.54	31.34	541.5
E3	159.1444-3	81–87	Buried valley	0.95	0.51	40.29	376
F1	168.1378-1	372–378	Miocene	3.24 (refresh)	0.53	46.12	609.5
F2	168.1378-2	341–345	Miocene	10.87 (refresh)	1.71	2.85	10510
F3	168.1378-3	208–214	Miocene	0.89	0.51	25.73	432.5
G1	168.1546-1	110–120	Miocene	0.67	0.50	42.57	346.5
G2	168.1546-2	74–84	Pleistocene/ Miocene	0.33	0.51	45.33	341.5

to a chloride concentration of 250 mg/L. The observed horizontal extent of the saltwater intrusion varies significantly from North to South (Figures 5 and 6). In the northern part of the area, where the topography is higher and hillier, the saltwater intrusion is limited due to the higher inland head. In contrast it extends up to 18 km inland at depths below 250 m in the buried valley further south in the marsh area. The extent of the saltwater intrusion simulated in scenarios A and B match the observed saline groundwater body similarly well in the shallow Quaternary aquifer system (Figures 5 and 6). However, in the deeper Miocene aquifer a satisfying match is only achieved with scenario B, while in scenario A the extent of the saltwater intrusion is underestimated in most places, except where the buried valley connects to the ocean (Figure 6, section $y = 6{,}087{,}800$ m). The differences in the match between the observed and simulated extent of saltwater intrusion in scenarios A and B show the sensitivity of the saltwater intrusion to different parameters. In scenario B, the higher horizontal and vertical hydraulic conductivities enhance both the horizontal intrusion of salt water (in all phases) and the downward infiltration as a result of the inundation during phase 2.

Simulated heads at the end of phase 3 match observed heads equally well in terms of mean error (ME) and root-mean-square error (RMSE) in both cases, with scenario A statistics of ME = −0.31 m and RMSE = 1.39 m and corresponding scenario B values of ME = 0.08 m and RMSE = 1.41 m. These are comparable to the ME = 0.19 m and RMSE = 1.36 m of the constant-density model (Meyer et al., 2018a).

4.2.3. Formation of Saltwater Intrusion During the Holocene

The formation of saltwater intrusion during phases 1 to 3 is explained by simulation results from scenario B at two representative cross sections and in a horizontal section at a depth of 255 m, Figure 7. Bear in mind that 3-D geological structures, resulting in 3-D flow, are difficult to illustrate. The vertical cross sections represent typical geological settings either through a buried valley (cross-section a) connecting the aquifer to the sea or without (cross-section b). Four mobile species represent “ocean” water (intruding horizon-

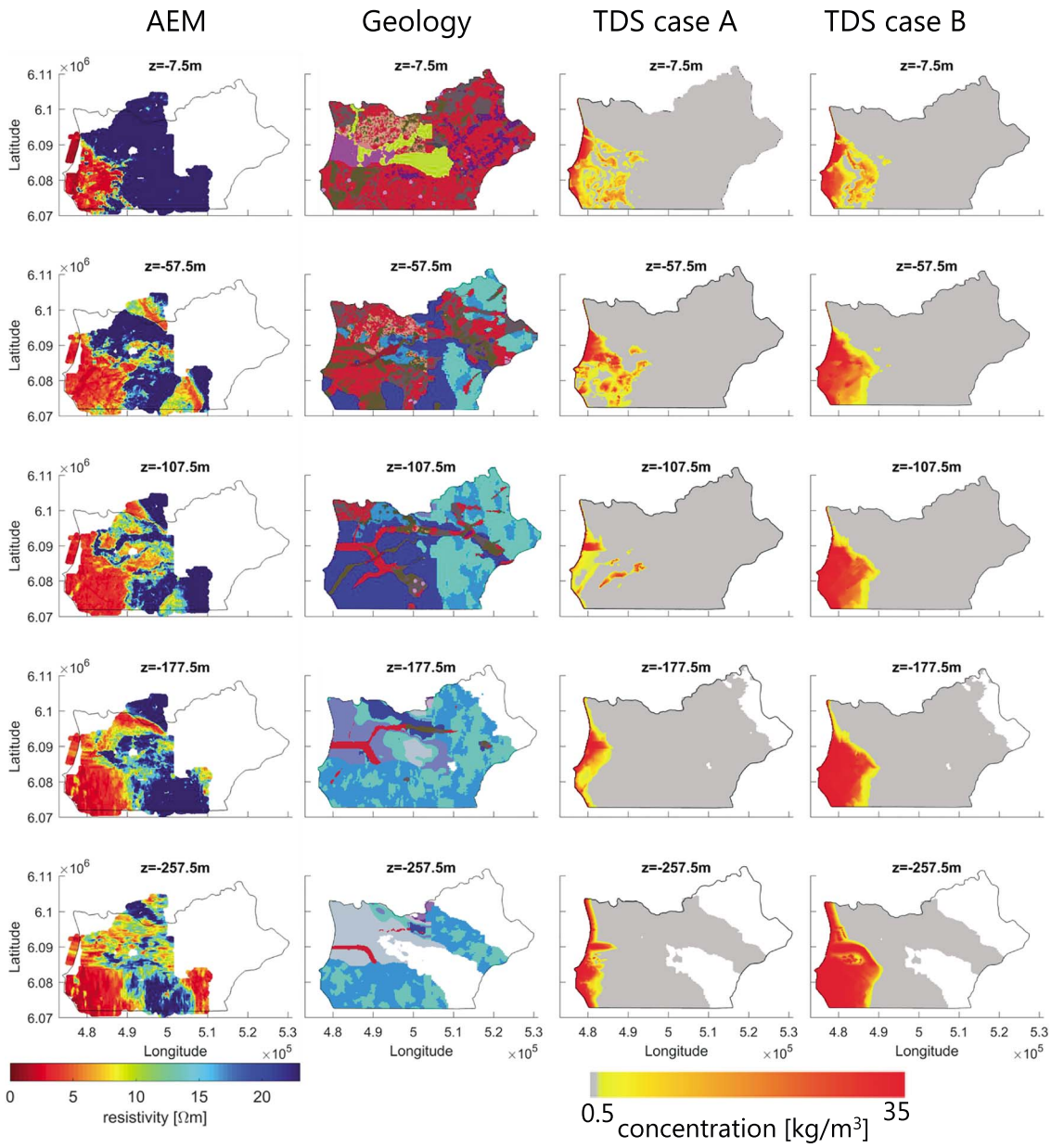

Figure 5. Horizontal sections through airborne electromagnetic (AEM) resistivity (first column), voxel representation of the geology (second column), total dissolved solids (TDS) simulation results of case A (third column), and B (fourth column) at different depths at the end of simulation phase 3. Description of geology as in Figure 6.

tally from the ocean boundary; illustrated by reddish colors), present in all phases; "transgression" (salt water seeping vertically from the flooded area; illustrated by bluish colors), present in phases 2 and 3; "local refreshing" (meteoric fresh water infiltrating vertically in the formerly inundated area; purple line) and "total refreshing" (meteoric fresh water infiltrating vertically in the entire area; black line), present only in phase 3.

In phase 1 the total mass of salt in the model (TDS, kg) increases as a result of horizontally intruding seawater (Figures 7 and 10a). Geological structures mainly control the progression of the saltwater intrusion. Where the permeable units connect to the ocean boundary, the seawater intrudes further inland. Where the buried valley connects to the ocean, it provides a preferential flow path for the intruding salt water and the formation of a more classical saltwater wedge (Figure 7, cross-section a). In other places, low-permeability clay units obstruct the intrusion and causes formation of saltwater intrusion to occur mainly in the deeper

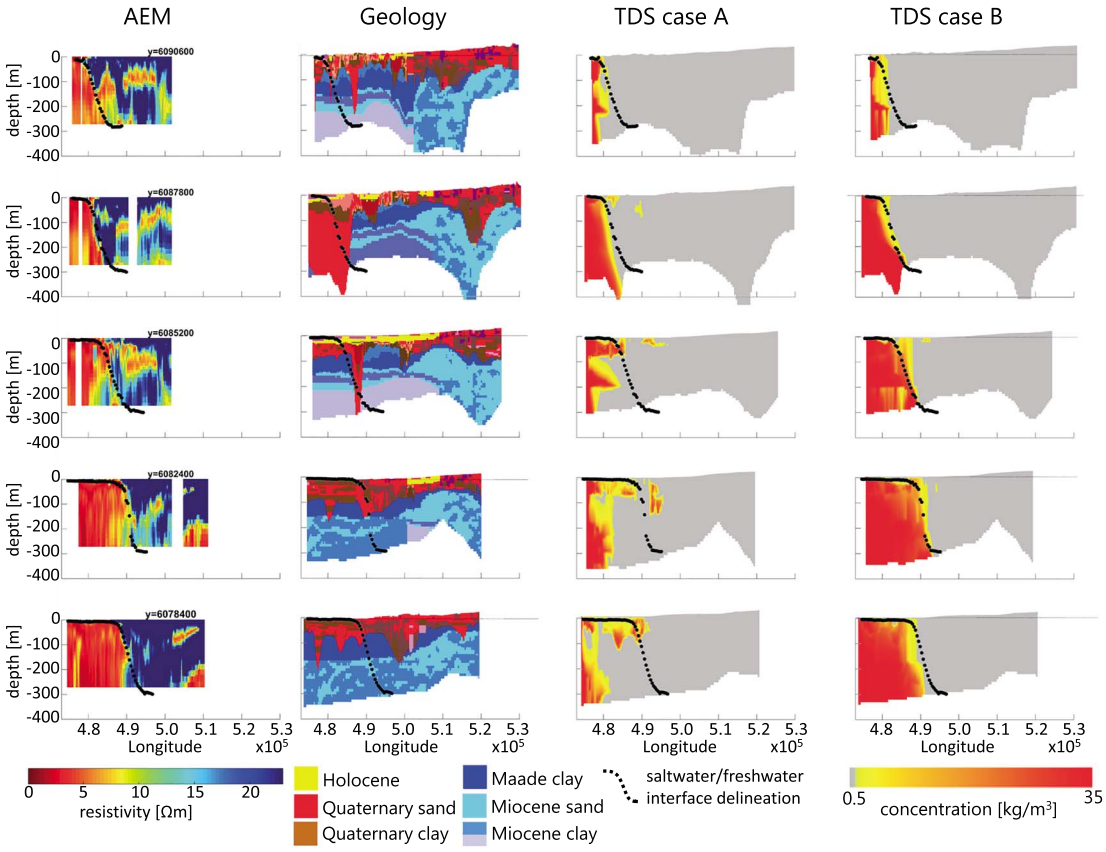

Figure 6. E–W cross sections through airborne electromagnetic (AEM) resistivity data (first column), voxel representation of the geology (second column), total dissolved solids (TDS) simulation results of case A (third column) and B (fourth column) at the end of simulation phase 3. The geological description is simplified in the legend, for a full description see Meyer et al. (2018a). Vertical exaggeration = 30.

Miocene aquifers (Figure 7, cross-section b). The high salt concentration at the bottom of the buried valley results from 3-D saltwater migration through the buried valley (compare with horizontal section, Figure 7). The horizontal extent of the 50% ocean TDS concentration reaches up to 14 km inland in the deep part of the buried valley, while in the rest of the marsh area it does not extent further than 10 km. Salt water mainly intrudes horizontally and leaks down into permeable layers further inland. Diffusion drives the spreading of the salt into the low-permeability clay units, where the advective flow is small, and delays the progression of saltwater intrusion. During the 2000 year period with inundation of the marsh area in phase 2, the deeper saltwater intrusion proceeds, but mainly in the south. Salt water infiltrates in the inundated area and increases the salinization rate (Figure 10) of the shallow groundwater. In the inundated area, free convection of vertical infiltrating salt water is observed (Figure 7, phase 2) in the permeable Quaternary sand aquifers, with formation of the typical fingering (e.g., between $x = 489{,}000$ m and $x = 495{,}000$ m) driven by the density differences forcing the salt water to seep down and the fresh groundwater to flow up. Seawater (represented by 50% seawater) originating from the transgression reaches locally to depths of 130 m below the surface (not shown). Fresh water from the Miocene aquifers, originating from the recharge areas in the east, flows upward in the buried valley, and hence limits the downward migration of transgression saltwater (Figure 7). Aquitards, either from Quaternary (e.g., Figure 7) or further below from Miocene (e.g., Figure 7), also impede the vertical infiltration of salt water, resulting in more horizontal spreading. As the deep Miocene and the shallow Quaternary aquifers are separated by the Maade formation in large parts of the coastal area, a two-layered saltwater intrusion is observed. In the shallow aquifers, the saltwater originates mostly from the transgression, while in the deeper aquifers the saltwater progression is driven by saltwater intrusion from the sea (classical intrusion). In between, the low permeable marine clay (Maade) delays the migration of the salt.

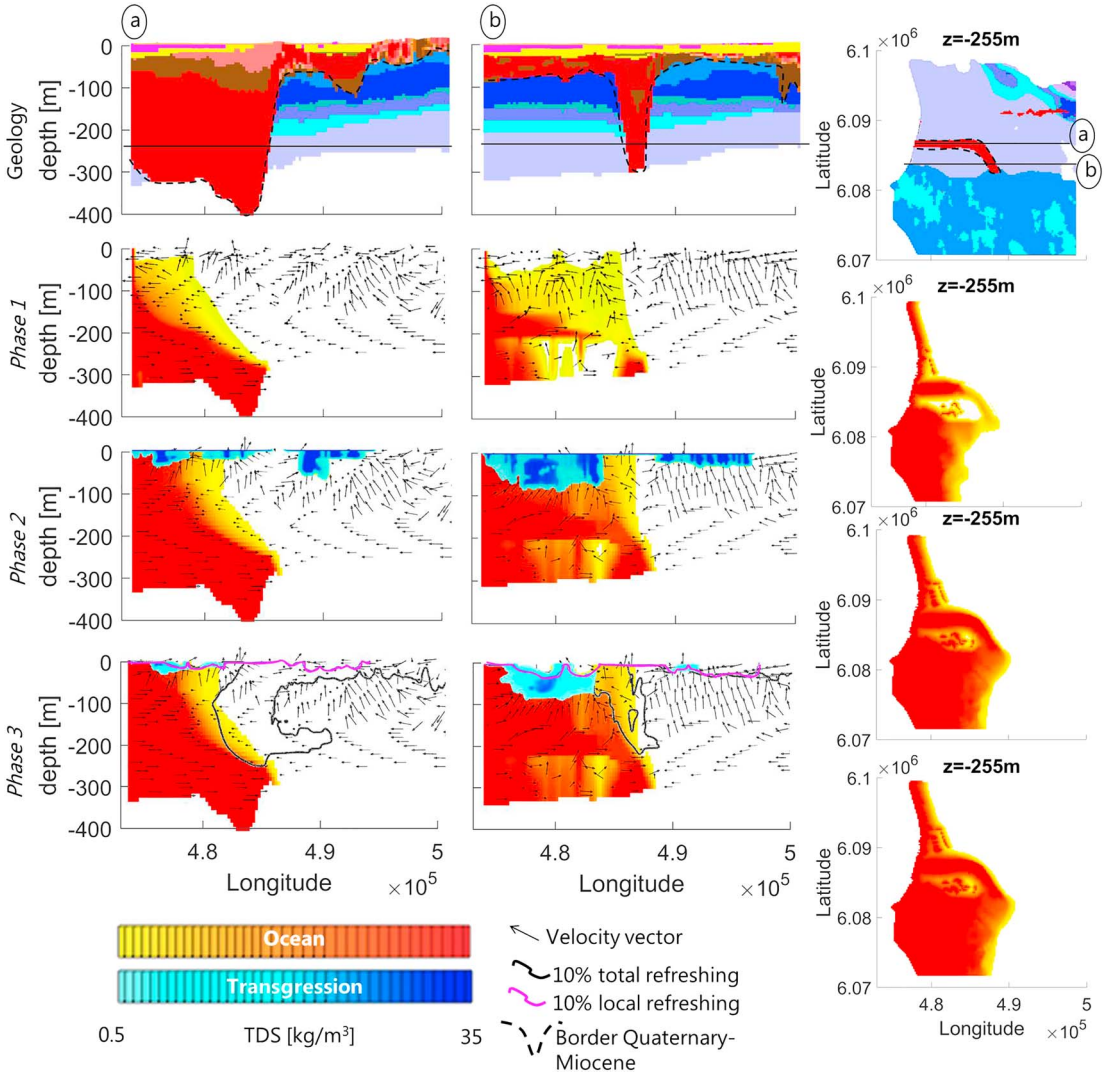

Figure 7. Formation of saltwater intrusion during phases 1 to 3 at two cross-sections (a) and (b) and a horizontal section at depth of 255 m below sea level. The boundary between Miocene and Pleistocene is shown with a dashed line, highlighting buried valleys in the geological sections. Description of geology as in Figure 6, vertical exaggeration = 30. The lateral intrusion is shown in red, while vertical transgression seawater is shown in blue (Phases 1–3). "Local refreshing" refers to meteoric water recharging only in the marsh area, "total refreshing" refers to meteoric water recharging over the total area.

With the construction of the dike ≈200 years BP, the area was protected from inundation and drains were established, at some location below sea level, to keep the groundwater below surface and allow agricultural use. This sudden change in boundary conditions first led to a steep decrease in TDS as a result of dropping in groundwater levels induced by the lowered drainage and replacement of transgression water ("transgression," Figure 10a) by infiltrating fresh water, the reassigned recharge in the marsh area. This is followed by an increase in total TDS as a result of enhanced seawater intrusion caused by the groundwater depression generated by the established drainage system ("ocean," Figure 10a). The saltwater intrusion reaches up to 18 km inland at the end of phase 3 (Figure 7 phase 3). In this phase 3, meteoric fresh water recharges, dilutes, and displaces transgression salt water. In the permeable Quaternary sand aquifers, locally recharging meteoric water (which means only recharge in the march area) reaches at some locations down to depths of 40 m below surface (Figure 7, phase 3, purple line), but with little infiltration in low-permeability sediments or where deep fresh water is upwelling. However, fresh water that infiltrates outside the marsh area reaches further down. For example, in the northern branch of the buried valley that acts as a preferential recharge area (Meyer et al., 2018a), fresh water reaches to depths of more than 200 m (Figure 7, phase 3, black line) before it moves upward along the freshwater-saltwater interface in the buried valley. This complicated salinization and refreshing system results in separate few-meter-thick freshwater lenses close to the surface

outside the buried valley. The drainage system induces a higher inland head gradient enforcing saltwater intrusion from the ocean boundary, while at the same time intensified upwelling of fresh water through buried valleys enhances the dilution and displacement of infiltrated salt water from the transgression (from phase 2). It is evident from Figure 10 that the system never reaches an equilibrium situation in any of the simulated phases.

4.2.4. Climate Change Scenarios

The impact of future climate change with an increase in recharge by 10% and a sea level rise by 85 cm over 200 years is compared relative to the extent of the present saltwater intrusion. Moreover, a simulation with steady boundary conditions over the same 200 years is used to distinguish changes in saltwater patterns caused by nonstationarity (as the system was not in equilibrium) from those explained by climate change. Figure 10a shows the evolution of salt from the different origins ("ocean" and "transgression") during the last 4200 years and for the future 200 years (Figure 10b), applying present-day conditions (referred to as "steady") and climate change conditions (referred to as "CC"). The relative increase in total load of TDS in the system after 200 years is 6.4% for the "CC" scenario compared to today and 2% compared to the "steady" scenario.

Figure 8 (top) shows the salt concentration, originating from the ocean boundary and the transgression, respectively, and the line of 10% total refreshing at the same cross sections as in Figure 7. Moreover, the differences in TDS concentrations between the "CC" and the "steady" scenarios are shown (Figure 8, bottom). While the toe position of the saltwater intrusion does not significantly advance further inland (in some locations up to 1 km), the transition zone between salt and fresh water moves considerably inland and higher TDS concentrations evolve in the upper aquifer and close to the surface. The increase in recharge enhances the fresh groundwater inflow into the buried valleys, pushing the intruding salt water outward and preventing its progression. This led to an increased upward flow in the buried valley. Transgression salt water is therefore increasingly displaced both by upward moving ocean water and by upward flowing fresh groundwater. Refreshing is enhanced in the buried valley at the border between the marsh and the upstream area, but reduced in the marsh area closer to the coast.

Figure 9 shows in a 3-D perspective the TDS concentration (a) today, (b) under climate change conditions, (c) the differences between climate change and today, and (d) the differences between climate change and the 200-year steady simulation. As a result of the increase in hydraulic head at the coast induced by the sea level rise, the salt water and the overlying fresh water are lifted up resulting in more salt in the shallow system. In the marsh area, where drains control the water table, this effect then produces a higher discharge through the drains. Hence, higher salinities reach closer to the surface and the thickness of freshwater lenses outside the buried valleys decrease, locally by up to 6 to 9 m. In the north, outside the marsh area, no saltwater intrusion was observed until today, but simulation results indicate that under climate change conditions salt water will start intruding into the high-permeable sand layers.

While the water balance components show only small changes in total TDS mass in the scenario with steady state boundary conditions (less than 3%), significant changes are observed in the climate change scenario. The inflow from the ocean boundary into the marsh area doubles and, at the same time, the direct groundwater discharge through the ocean boundary is reduced by 75%. The amount of water captured by the drains increases by 14% in the marsh area. Outside the marsh area, the inflow from the ocean increases by 13%, while the discharge to the ocean decreases by 19% and the discharge through drains increases by 13% and through rivers by 5%.

5. Discussion

By combining a density-driven flow and transport model with geophysical and hydrogeochemical data, new insights are obtained about saltwater intrusion mechanisms at regional scale during the Holocene and in the future in a hydrologically and geologically complex coastal environment. In the following, to demonstrate the applicability of the methods used in this study, the prospects and challenges of the modeling approach and uncertainty of available data will be discussed. Additionally, the initial questions about the (i) origin

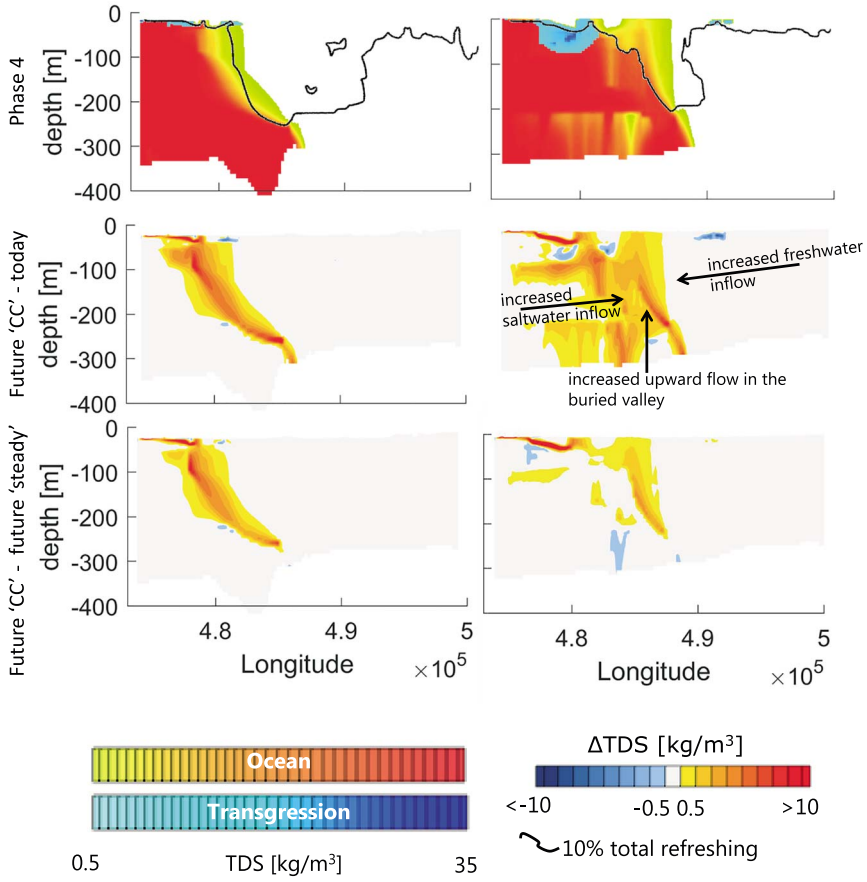

Figure 8. (top) Seawater intrusion in 200 years under climate change conditions (10% increase in recharge and 0.85 m sea level rise). (middle) Change in salt concentration between the 200-year climate change scenario and today. (bottom) Change in salt concentration between the 200 years climate change scenario and the 200-year "steady" scenario. Vertical exaggeration = 30. The cross sections refer to the same profiles as in Figure 7.

and (ii) dynamics of the salt water, (iii) the role of geological features, and (iv) the possible impact of future sea level rise on the saltwater intrusion are addressed.

5.1. Modeling Approaches and Uncertainties

A satisfactory simulation of the groundwater system is obtained, when considering the uncertainties on the observed saltwater/freshwater interface, the uncertainties associated with the geological model, as well as the flow and transport models. This is clear from the good match between the observed and simulated heads as well as the match between the freshwater/saltwater interface based on AEM data and the simulated saltwater intrusion. The overall acceptable match with the AEM data is to be credited to the regional, highly parameterized, hydrogeological model where parameters and their uncertainties were estimated using regularized inverse modeling (Meyer et al., 2018a), representing local-scale heterogeneities, together with the consideration of past conditions (Hughes et al., 2009) using a phase-wise approach (1–3) (Delsman et al., 2014).

The extent of the saltwater intrusion and the time it needs to develop is very sensitive to the parameterization and hydraulic conductivities and less sensitive to dispersion, recharge, and sea level. This is in line with Webb and Howard (2011) who discovered that a high ratio between hydraulic conductivity and recharge as well as a high effective porosity enhanced saltwater intrusion extent, and it took longer to reach equilibrium. In a heterogeneous system with highly parameterized hydraulic properties, including spatially distributed recharge and porosity, finger formation instabilities also vary over space and time and thus, slow down the establishment of equilibrium conditions (Simmons et al., 2001). Our simulation cases (A–E) were also not in equilibrium at the end of phase 3 (present day).

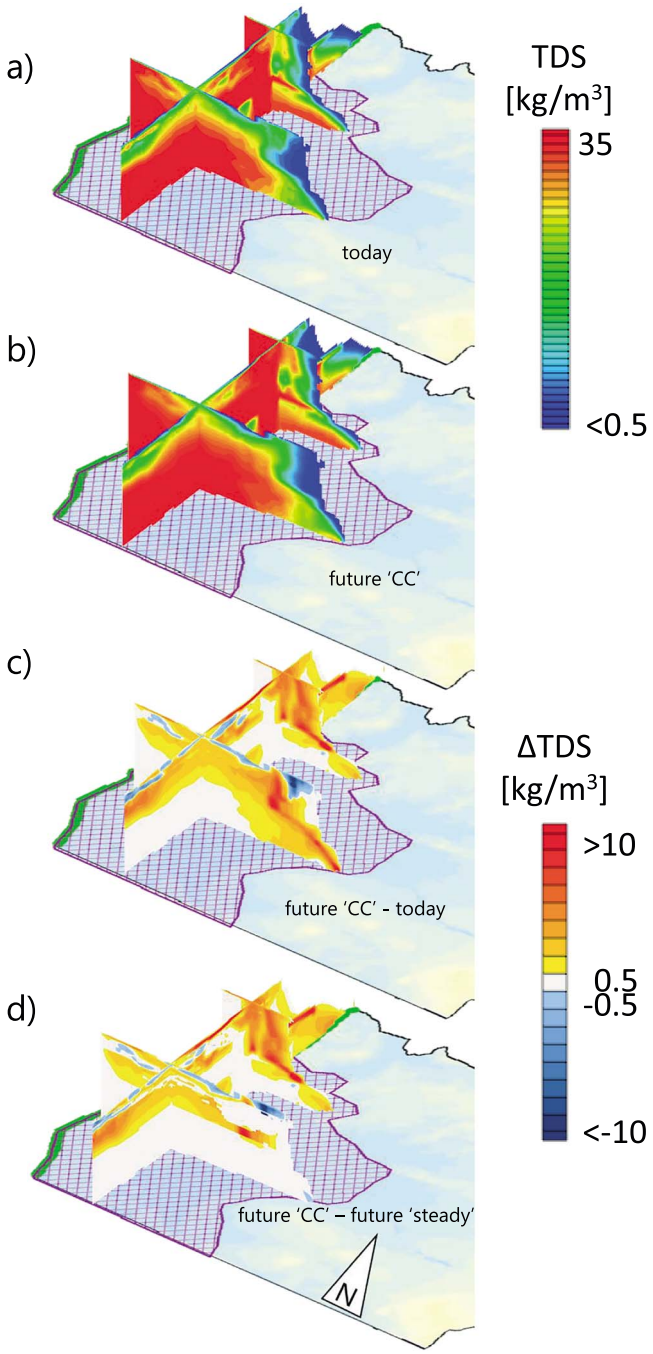

Figure 9. (a) Seawater intrusion today; (b) under climate change conditions in 200 years; (c) difference in salt concentration between the 200-year climate change scenario and today (red = salinization, blue = refreshing); (d) difference in salt concentration between the 200-year climate change scenario and a 200-year simulation with steady conditions. Vertical exaggeration = 20.

The results of the sensitivity runs show that, given the evidence from AEM, it cannot be distinguished between scenarios A and C–E, each of these appear equally unlikely. The changes based on these cases affect the model significantly less than changes in the calibrated parameter space (scenario A vs. B). Two sets of parameters were tested (scenarios A and B), representing "best estimated" hydraulic parameters (scenario A) and "high hydraulic conductivities" using the corresponding upper uncertainty limits (scenario B). Meyer et al. (2018a), using a constant-density model, showed that both models match hydraulic head observations equally well. In comparison with the AEM data, scenario A underpredicts the extent of the saltwater intrusion significantly. However, scenario B, representing a more permeable system, matches the extent of

the saltwater intrusion much better. Following Shoemaker (2004), it was realized that estimated hydraulic parameters based on calibration against head observations and discharge would not necessarily result in an accurate simulation of concentrations in a density-dependent solute transport model. This is particularly true in this study, where available head observations were not equally distributed over the investigation area with only few head data near the saline groundwater body. However, key observation in this study is that by quantifying uncertainty derived from a highly parameterized regularized inverse model based on head and age observations, it is possible to capture observed saltwater intrusion patterns using realistic parameters without compromising the flow calibration results.

Despite the promising modeling results, some limitations and simplifications need to be addressed. Walther et al. (2017) recently showed that a sloping seabed would shift the transition zone seaward and hence reduce the onshore extent of the saltwater intrusion. In conditions similar to those in this study, this would be only of minor relevance. Compared to other uncertainties in the present modeling study, for example, seaward extent of the Miocene aquitard, the use of a vertical sea boundary seems reasonable. Neglecting the geographical and geological changes (i.e., paleo-evolution by sedimentation of Holocene deposits and variation in the river system) and using a simplified description of historic sea level add to the uncertainties (Meyer et al., 2018a, 2018b). We are not able to address this issue, but it is the scope of future work as Delsman et al. (2014) and Hughes et al. (2009) showed the importance of accounting for paleo-evolution of the hydraulic system in the Holocene and before. Less geological information were available for the German part of the study area and hence the description of the geology in the German part was less detailed than in the remaining area. This had implications for the parameterization and simulation primarily for the Miocene sections (patchy and partly disconnected Miocene sand lenses). To compensate for these inaccuracies a relatively high Kh of Lower Miocene clay (in the German part) was estimated compared to the expected value for this unit.

The use of AEM data showed a promising potential by providing a regional areal coverage and a continuous depth interpretation of the present-day saltwater distribution. However, a quantitative comparison between AEM and simulated salt concentrations, which would be desirable, was not possible as the relation between formation resistivity, observed by AEM, and porewater chloride concentration, simulated by the model, is not trivial (and additional information, e.g., about formation factors was not available). In future studies, it could be interesting to use AEM data in combination with borehole observations of chloride concentrations (Siemon et al., 2009), such that full autocalibration of saltwater intrusion models could be carried out to estimate hydraulic parameters. Unfortunately, this is challenged by high uncertainties and ambiguity associated with the translation of AEM data into chloride concentrations, especially in highly heterogeneous clay-rich environments (Siemon et al., 2009). Delsman et al. (2018) demonstrate a probabilistic approach to derive categories of salt concentration from AEM data, which could in the future be of value for constraining saltwater intrusion models. Additionally, the long computer run times for simulating regional saltwater intrusions (each run in this study took ≈3 days on a 12 core Intel Xeon CPU E5-1650 3.5GHz (64GB RAM) PC) are a challenge.

5.2. Origin and Dynamics of Salt Water

The saltwater intrusion simulation results partly underpin the hypotheses of Jørgensen et al. (2012) about the Holocene origin of the salt water and suggest that most of the present saline water intruded the system laterally from the ocean boundary (95% of the total salt present in the system today). The intrusion was induced by Holocene postglacial sea level rise. Transgression water, infiltrating vertically in the low-lying areas during phase 2, only contributes to a small extent (about 4%) to the present mass of salt in the shallow aquifers. Clay deposits impeded its further vertical infiltration, as has been shown in other cases (Simmons et al., 2001), but transgression water is nevertheless important for the salinization of the shallow aquifers. The current setting is different from the Dutch systems (e.g., Delsman et al., 2014), where transgression water was the major source of salt in the high-permeable coastal aquifers. In such systems, kilometer-wide dune landscapes between the polders and the ocean and a relatively high gradient in topography allow the formation of Ghyben-Herzberg-type freshwater lens that prevent ocean water from intruding into the shallow coastal aquifers.

5.2.1. Origin of Inland Salt

The relatively high chloride concentrations in the wells far from the coast (wells C1, C2, C3, D1, D2, and F2) cannot be explained by saltwater intrusions during the Holocene (as simulations do not show salt water this far inland). Diffusion of remnant salt in the porewater of low-permeability Miocene clay formations could be

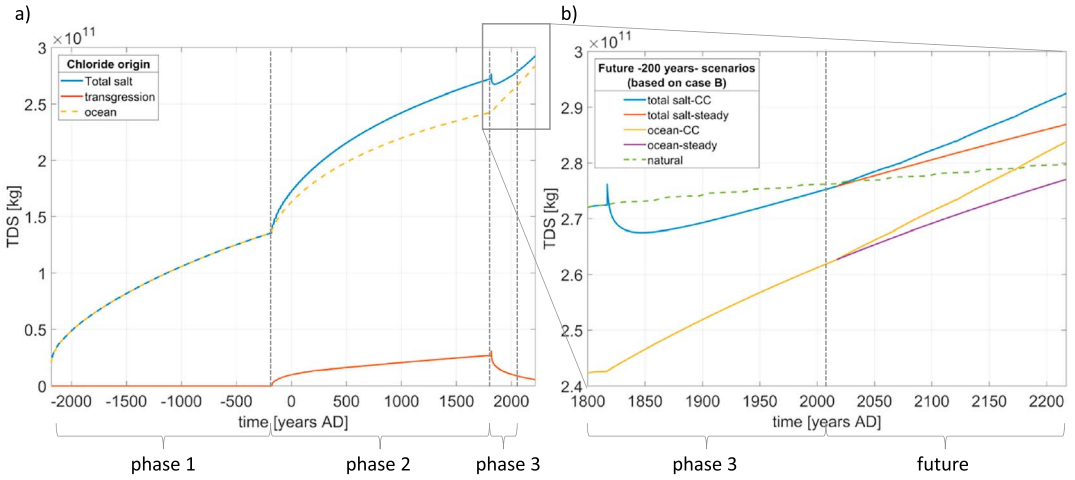

Figure 10. (a) Change of total amount of total dissolved solids (TDS) over time during the simulated phases 1–3 and (b) for the future scenario for the "total salt" (transgression + ocean), "ocean salt" (intruding horizontally from the coastal boundary) and "transgression" (infiltrating vertically in the flooded area). Hereby, "steady" refers to the case where the present boundary conditions are used during the 200-year future simulation and "CC" refers to climate change conditions (10% increase in recharge and a relative sea level rise of 85 cm); "natural" shows the TDS evolution if no dike and drainage would have been established (400 years continuation of phase 2).

the source of the salt. This hypothesis is supported by induction log data at well F and and at the well with the DGU number 166.711 (locations are shown in Figure 1; data available from GERDA, http://www.gerda.dk). The induction logs in the low-permeability Miocene clay formations show outward directed diffusive gradient which could indicate salt leaching into the surrounding aquifers. Whether the salt comes from the time of deposition of these marine deposits or was flushed into it during transgressions in the pre-Holocene interglacial periods, when shallow seas covered the area (e.g., Eemian sea), cannot be distinguished. The hypothesis of remnant saline porewater is supported by the fact that the well screens in question are located deep in the buried valley below a thick Pleistocene clay unit (well location C), and close to Miocene clay units (well locations C, D, F). Table 2 also shows that at these well screens the ^{14}C concentrations is very low, which point to high groundwater ages (see Meyer et al., 2018b for more details). This observation disagrees with Jørgensen et al. (2012), who speculated that the aquifers have been completely flushed during the Weichselian. It could be argued that the remnant marine porewater should have been washed out (Larsen et al., 2017) given the time since deposition. One explanation that this is not the case could be that the region was under permafrost conditions during the Weichselian, even though not covered by the glacier itself. The permafrost would then have acted as an impervious layer (Sterckx et al., 2017), limiting deeper advective and diffusive flow and transport, and remnant salt, from, for example, the Eemian sea, would thus not have been flushed out completely from low-permeability Miocene sediments. With the onset of permafrost thawing, enhanced deeper flow through shallower Pleistocene permeable sediments including buried valleys could have accelerated the flushing of salt residuals from these sediments, while higher salinity could have been preserved in the porewater of low-permeability Miocene clay. The distribution and concentration of remnant salt is unknown and associated with high uncertainties. Nevertheless, a test scenario was conducted with parameter set A and an initial salt concentration of 5 kg/m^3 in all Miocene clay units (the results are not shown, for brevity). The results support the hypothesis of that if remnant salt was present in the system after the Weichselian glaciation, it might be still present today. However, the results do not match the AEM data. Because of the high uncertainties associated with paleo salt water distribution and paleo hydraulic conditions, no attempt was undertaken to further explore this in this simulation study.

5.2.2. System State

Another question raised by Jørgensen et al. (2012) related to the system dynamics and its state could be clarified by the model scenario analysis. Refreshing inside the marsh area, in response to flood prevention by dike construction is restricted to the uppermost few meters, locally to tens of meters, of the shallow aquifer. Locally recharging meteoric water dilutes former transgression water and generates several separated freshwater lenses (De Louw et al., 2011). In the deeper aquifers, continuous salinization is induced by the drainage system, while freshwater inflow from outside the marsh area counteracts the saltwater progression.

Because salt migration and mixing respond slowly, particularly in confined aquifers and with distance from the coast (Hughes et al., 2009), the system has not reached an equilibrium during any of the simulated phases before new instabilities were introduced by new boundary conditions (Figure 10). Additionally, simulation results imply that equilibrium in phase 2 might have been reached within ≈2500 years (Figure 10, natural steady conditions of phase 2), given steady boundary conditions, but land reclamation reestablished nonstationarity which is further intensified under climate change conditions (Figure 10).

5.3. Structural Influence

Structural elements and water/land management are essential features that influenced flow and transport dynamics and, hence, the formation of the present saltwater pattern in the investigation area.

The special role of the extensive marine clay (Maade formation) for the flow system was already revealed by simulations of Meyer et al. (2018a). Over large areas, this unit confines the lower Miocene aquifers from the upper Quaternary aquifer systems and generates artesian conditions in the Miocene sand formations (evident at borehole screens A1, A2, B1, B2, C1, D1, D2, and F1–F3). Jørgensen et al. (2012) proposed several explanations about the flow system in the Miocene sand aquifer and the role of the Maade formation in order to understand resistivity patterns in the AEM data. The results of the present study add confidence to the interpretation of the Miocene sand aquifer as an active flow system fed by recharge in the very east of the catchment and confined by the Maade formation in the west. Naturally, the permeable Miocene sand formations constitute locations of enhanced lateral intrusion of saline water from the ocean boundary, while the Maade clays delay its progression, as salinization of the clay mostly is driven by diffusion. The importance of accounting for flow and transport in three dimensions and representing 3-D (hydro-) geological elements (Hughes et al., 2009) in order to explain the occurrence and formation of saltwater pattern is emphasized in this study. For example, flow in the buried valley is angular to the main flow direction where it follows the direction of the buried valley, and salt water is transported in the deep part of the buried valley (e.g., Figure 7, cross-section b, at a depth of 250 to 300 m and $x = 489{,}000$ m). Clay lenses cause a reversal and even dispersal of flow directions locally. During transgression, mixed convection (Simmons et al., 2001), driven by advection and buoyancy forces formed large-scale salt fingering in the high-permeable sediments close to the surface. Where low-permeability units extend horizontally, they form barriers to further vertical infiltration similar to those described by Simmons et al. (2001).

The head differences between the deep Miocene and the shallow Pleistocene aquifer systems force groundwater to flow upward. This exchange preferably occurs in the buried valleys, filled with coarse permeable sediments, that cut through the Maade formation and connect the two aquifer systems. The upward flow is large enough to repress the convective infiltration of denser transgression water in the buried valley (e.g., Figure 7 cross-section b, during phase 2).

Land reclamation and establishment of dikes and drains, controlling the groundwater table, induced a depression in the groundwater level in the marsh area. In this way, higher lateral and vertical flows are generated and result in an inland progression of the salt water and in an uplift of the salt water. Thus, increased salinization of the upper aquifer takes place while enhanced upwelling of fresh water in the vicinity of the buried valleys dilutes the salt water from the bottom. The initialized local refreshing concomitant with the land reclamation formed separated shallow freshwater lenses and replaced and diluted formerly transgression water, but did not contribute to a refreshing of the deep aquifer system.

5.4. Climate Change

Two future scenarios, simulated over a period of 200 years, distinguish the effect of nonstationarity (Hughes et al., 2009) of the present system from those induced by climate change conditions on the salinization of the system. Similar to the Dutch system (Oude Essink et al., 2010), future salinization in the deeper aquifer inside the marsh area is more related to nonstationarity of the present system than to climate change effects, while in the upper aquifer, in the buried valley and north of the marsh area, salinization is intensified by climate change (Figure 9). Under climate change conditions, the toe position in the deep aquifer will not significantly migrate landward when the border of the drained area is reached. The saltwater intrusion will rather extend into low-permeability formations and move upward caused by the increased flux from the coastal boundary (twice as high compared to today). On the other hand, enhanced freshwater upwelling caused by increasing groundwater recharge will counteract the intruding salt water.

The deterioration of water quality close to the surface together with an increase in drain discharge has direct consequences for water quantity and quality, for agriculture and ecology. Increasing drain discharge (by 13%) requires that water management is adapted, for example, increased pumping into the Vidå river. An elevated salinity evokes ramifications for agricultural yield and diversity of ecological communities (Pitman & Läuchli, 2002).

6. Conclusions

Two research challenges were addressed in this study. The first one concerns the understanding of the development of a large-scale saltwater intrusion and questions raised by Jørgensen et al. (2012). The second one relates to the technical implementation, integration of available data and the model setup. Sea level variations have recurrently changed the face of the Earth and are closely linked to global climate and geological controls. When sea level rises, aquifers in low-lying coastal areas are threatened by contamination of seawater. In order to better predict (ongoing) salinization of coastal aquifers, initial salt concentrations, induced by past hydraulic conditions, coastal geology, and relative sea level changes have to be taken into account. Implementing a detailed heterogeneous (hydro-)geology on a regional scale allowed to reproduce saltwater patterns similar to those observed with AEM data. Such data are valuable for validating modeling results and constraining the parameter field. Specifically, upper uncertainty limits of hydraulic parameters (Meyer et al., 2018a) were needed to produce a saltwater intrusion over long time scales that matched AEM interpretations satisfactorily. The simulations were conducted in three phases, and changes in sea level and land management were accounted for. However, simulations of postglacial saltwater intrusion could not explain elevated salinities in inland wells. Instead, remnant salt water might have been present in the low permeable formations, which now diffuses into the local aquifers. The simulation results suggest that the present salt water in the coastal aquifers is mainly of seawater origin, intruded horizontally in response to the postglacial sea level rise. To a smaller extent, limited to the shallow aquifers, it was caused by Holocene transgression since vertical infiltrations into deeper aquifers were impeded by low-permeability formations and groundwater upwelling in the buried valleys.

Our modeling results show that the groundwater flow and transport dynamics, driven by the relative sea level rise, did not reach an equilibrium during the past 4200 years. Thus, a longer time is required to reach equilibrium in a density-driven heterogeneous groundwater system, even under undisturbed, natural conditions. Nonequilibrium is maintained by anthropogenic activity, such as land reclamation in combination with drainage, and will be intensified by future relative sea level rise caused by climate change and land subsidence. Salinization of the deep Miocene aquifers will be primarily a result of nonstationarity, induced by land reclamation and drainage about 200 years ago, while in the shallower aquifer salinization will be primarily caused by the relative sea level rise.

The approaches outlined in this study give directions for similar modeling studies. Large-scale models with realistic geology can be paired with stepwise historical evolution of the landscape to reproduce current saline groundwater bodies. This gives confidence in using these types of models for the predictions of future contamination.

Acknowledgments
The authors acknowledge Geocenter Denmark for funding the study. We acknowledge the Master thesis of Anne Rose Aagaard who delineated the freshwater/saltwater interface and thank Flemming Jørgensen for the interpretation of the AEM data and discussions. The authors thank the Editors and three anonymous reviewers for their comments that helped to improve the paper substantially. The data used in this study are available from the national databases for geophysical data GERDA (http://www.geus.dk/produkter-ydelser-og-faciliteter/data-og-kort/national-geofysisk-database-gerda/) and geological data JUPITER (https://www.geus.dk/produkter-ydelser-og-faciliteter/data-og-kort/national-boringsdatabase-jupiter/).

References

Abarca, E. (2006). Seawater intrusion in complex geological environments. Tech. Univ. Catalonia, UPC PhD Thesis 154, http://www.tdx.cat/TDX-0222107-105833

Appelo, C. A. J., & Postma, D. (2005). Geochemistry, groundwater and pollution. Balkema Publishers, Amsterdam, ISBN 041536 428 0.

Behre, K.-E. (2007). A new Holocene sea-level curve for the southern North Sea. *Boreas*, *36*, 82–102. https://doi.org/10.1080/03009480600923386

Carrera, J., Hidalgo, J. J., Slooten, L. J., & Vázquez-Suñé, E. (2010). Computational and conceptual issues in the calibration of seawater intrusion models. *Hydrogeology Journal*, *18*, 131–145. https://doi.org/10.1007/s10040-009-0524-1

Chang, S. W., Clement, T. P., Simpson, M. J., & Lee, K.-K (2011). Does sea-level rise have an impact on saltwater intrusion? *Advances in Water Resources*, *34*, 1283–1291. https://doi.org/10.1016/ j.advwatres.2011.06.006

Church, J. A., Clark, P. U. A., Gregory, J. M., Jevrejeva, S., Levermann, A., Merrifield, M. A., et al. (2013). Sea level change. In T. F. Stocker et al. (Eds.), *Climate change 2013: The physical science basis. Contribution of Working Group I to the Fifth Assessment Report of the Intergovernmental Panel on Climate Change* (pp. 2013). USA: Cambridge University Press Cambridge, United Kingdom and New York, NY.

De Louw, P. G. B., Eeman, S., Siemon, B., Voortman, B. R., Gunnink, J., Van Baaren, E. S., & Oude Essink, G. H. P. (2011). Shallow rainwater lenses in deltaic areas with saline seepage. *Hydrology and Earth System Sciences*, *15*, 3659–3678. https://doi.org/10.5194/hess-15-3659-2011

Delsman, J. R., Hu-a-ng, K. R. M., Vos, P. C., de Louw, P. G. B., Oude Essink, G. H. P., Stuyfzand, P. J., & Bierkens, M. F. P. (2014). Paleo-modeling of coastal saltwater intrusion during the Holocene: An application to the Netherlands. *Hydrology and Earth System Sciences*, *18*, 3891–3905. https://doi.org/10.5194/hess-18-3891-2014

Delsman, J., Van Baaren, E. S., Siemon, B., Dabekaussen, W., Karaoulis, M. C., Pauw, P., et al. (2018). Large-scale, probabilistic salinity mapping using airborne electromagnetics for groundwater management in Zeeland, the Netherlands. *Environmental Research Letters*, *13*. https://doi.org/10.1088/1748-9326/aad19e

Doherty, J. (2016). Model-independent parameter estimation I. Watermark numerical computing, 366, http://www.pesthomepage.org/Downloads.php.

Faneca Sànchez, M., Gunnink, J. L., Van Baaren, E. S., Oude Essink, G. H. P., Siemon, B., Auken, E., et al. (2012). Modelling climate change effects on a Dutch coastal groundwater system using airborne electromagnetic measurements. *Hydrology and Earth System Sciences*, *16*, 4499–4516. https://doi.org/10.5194/hess-16-4499-2012

Gelhar, L. W., Welty, C., & Rehfeldt, K. R. (1992). A critical review of data on field-scale dispersin in aquifers. *Water Resources Research*, *28*, 1955–1974. https://doi.org/10.1029/92WR00607

GERDA (http://www.gerda.dk). Danish national database for geophysical data.

GEUS (http://www.geus.dk/UK/data). JUPITER—Danish national database for geological and hydrological data.

Hansen, J. M., Aagaard, T., & Binderup, M. (2012). Absolute sea levels and isostatic changes of the eastern North Sea to central Baltic region during the last 900 years. *Boreas*, *41*, 180–208. https://doi.org/10.1111/j.1502-3885.2011.00229.x

Henriksen, H. J., Troldborg, L., Nyegaard, P., Sonnenborg, T. O., Refsgaard, J. C., & Madsen, B. (2003). Methodology for construction, calibration and validation of a national hydrological model for Denmark. *Journal of Hydrology*, *280*, 52–71. https://doi.org/10.1016/S0022-1694(03)00186-0

Hinsby, K., Condesso de Melo, M. T., & Dahl, M. (2008). European case studies supporting the derivation of natural background levels and groundwater threshold values for the protection of dependent ecosystems and human health. *The Science of the Total Environment*, *401*, 1–20. https://doi.org/10.1016/j.scitotenv.2008.03.018

Hughes, J. D., Vacher, H. L., & Sanford, W. E. (2009). Temporal response of hydraulic head, temperature, and chloride concentrations to sea-level changes, Floridan aquifer system, USA. *Hydrogeology Journal*, *17*, 793–815. https://doi.org/10.1007/s10040-008-0412-0

Jørgensen, F., & Sandersen, P. B. E. (2006). Buried and open tunnel valleys in Denmark—Erosion beneath multiple ice sheets. *Quaternary Science Reviews*, *25*, 1339–1363. https://doi.org/10.1016/j. quascirev.2005.11.006

Jørgensen, F., Scheer, W., Thomsen, S., Sonnenborg, T. O., Hinsby, K., Wiederhold, H., et al. (2012). Transboundary geophysical mapping of geological elements and salinity distribution critical for the assessment of future sea water intrusion in response to sea level rise. *Hydrology and Earth System Sciences*, *16*, 1845–1862. https://doi.org/10.5194/hess-16-1845-2012

Kaleris, V., Lagas, G., Marczinek, S., & Piotrowski, J. A. (2002). Modelling submarine groundwater discharge: An example from the western Baltic Sea. *Journal of Hydrology*, *265*, 76–99. https://doi.org/10.1016/S0022-1694(02)00093-8

Karan, S., Kidmose, J., Engesgaard, P., Nilsson, B., Frandsen, M., Ommen, D. A. O., et al. (2014). Role of a groundwater-lake interface in controlling seepage of water and nitrate. *Journal of Hydrology*, *517*, 791–802. https://doi.org/10.1016/j.jhydrol.2014.06.011

Karlsson, I. B., Sonnenborg, T. O., Jensen, K. H., & Refsgaard, J. C. (2014). Historical trends in precipitation and stream discharge at the Skjern River catchment, Denmark. *Hydrology and Earth System Sciences*, *18*, 595–610. https://doi.org/10.5194/hess-18-595-2014

Kehew, A. E., Piotrowski, J. A., & Jørgensen, F. (2012). Tunnel valleys: Concepts and controversies—A review. *Earth-Science Reviews*, *113*, 33–58. https://doi.org/10.1016/j.earscirev.2012.02.002

Langevin, C. D., Thorne Jr., D. T., Dausman, A. M., Sukop, M. C., & Guo, W. (2007). SEAWAT version 4: A computer program for simulation of multi-species solute and heat transport. *Specification for the US Geological Survey Historical Topographic Methods B.*, *6*, 39.

Larsen, F., Tran, L. V., Van Hoang, H., Tran, L. T., Christiansen, A. V., & Pham, N. Q. (2017). Groundwater salinity influenced by Holocene seawater trapped in incised valleys in the Red River delta plain. *Nature Geoscience*, *10*, 376–381. https://doi.org/10.1038/ngeo2938

Meyer, R., Engesgaard, P., Hinsby, K., Piotrowski, J. A., & Sonnenborg, T. O. (2018b). Estimation of effective porosity in large-scale groundwater models by combining particle tracking, auto-calibration and ^{14}C dating. *Hydrology and Earth System Sciences*, *22*, 4843–4865. https://doi.org/10.5194/hess-22-4843-2018

Meyer, R., Engesgaard, P., Høyer, A.-S., Jørgensen, F., Vignoli, G., & Sonnenborg, T. O. (2018a). Regional flow in a complex coastal aquifer system: Combining voxel geological modelling with regularized calibration. *Journal of Hydrology*, *562*, 544–563. https://doi.org/10.1016/j.jhydrol.2018.05.020

Michael, H. A., Russoniello, C. J., & Byron, L. A. (2013). Global assessment of vulnerability to sea-level rise in topography-limited and recharge-limited coastal groundwater systems. *Water Resources Research*, *49*, 2228–2240. https://doi.org/10.1002/wrcr.20213

Mulligan, A. E., Evans, R. L., & Lizarralde, D. (2007). The role of paleochannels in groundwater/seawater exchange. *Journal of Hydrology*, *335*, 313–329. https://doi.org/10.1016/j.jhydrol.2006. 11.025

Nishikawa, T., Siade, A. J., Reichard, E. G., Ponti, D. J., Canales, A. G., & Johnson, T. A. (2009). Stratigraphic controls on seawater intrusion and implications for groundwater management, Dominguez Gap area of Los Angeles, California, USA. *Hydrogeology Journal*, *17*, 1699–1725. https://doi.org/10.1007/s10040-009-0481-8

Oude Essink, G. H. P. (2001). Salt water intrusion in a three-dimensional groundwater system in the Netherlands: A numerical study. *Transport in Porous Media*, *43*, 137–158. https://doi.org/10.1023/A:1010625913251

Oude Essink, G. H. P., Van Baaren, E. S., & De Louw, P. G. B. (2010). Effects of climate change on coastal groundwater systems: A modeling study in the Netherlands. *Water Resources Research*, *46*, W00F04. https://doi.org/10.1029/2009WR008719

Pauw, P., De Louw, P. G. B., & Oude Essink, G. H. P. (2012). Groundwater salinisation in the Wadden Sea area of the Netherlands: Quantifying the effects of climate change, sea-level rise and anthropogenic interferences. *Netherlands Journal of Geosciences-Geologie En Mijnbouw*, *91*, 373–383. https://doi.org/10.1017/S0016774600000500

Piotrowski, J. A. (1994). Tunnel-valley formation in northwest Germany—Geology, mechanisms of formation and subglacial bed conditions for the Bornhöved tunnel valley. *Sedimentary Geology*, *89*, 107–141. https://doi.org/10.1016/0037-0738(94)90086-8

Piotrowski, J. A. (2007). Groundwater under ice sheets and glaciers. In P. G. Knight (Ed.), *Glacier Science and Environmental Change* (pp. 50–60). Maldon, MA Oxford: Blackwell Publishing. https://doi.org/10.1002/9780470 750636.ch9

Pitman, M. G, & Läuchli, A. (2002). Global impact of salinity and agricultural ecosystems. In A. Läuchli & U. Lüttge (Eds.), *Salinity: Environment - Plants - Molecules* (pp. 3–20). Dordrecht: Springer. https://doi.org/10.1007/0-306-48155-3

Post, V., & Abarca, E. (2009). Preface: Saltwater and freshwater interactions in coastal aquifers. *Hydrogeology Journal*, *18*, 1–4. https://doi.org/10.1007/s10040-009-0561-9

Rasmussen, J., Sonnenborg, T. O., Stisen, S., Seaby, L. P., Christensen, B. S. B., & Hinsby, K. (2012). Climate change effects on irrigation demands and minimum stream discharge: impact of bias-correction method. *Hydrology and Earth System Sciences*, *16*, 4675–4691. https://doi.org/10.5194/hess-16-4675-2012

Shoemaker, W. B. (2004). Important observations and parameters for a salt water intrusion model. *Ground Water*, *42*, 829–40. https://doi.org/10.1111/j.1745-6584.2004.t01-2-.x

Siemon, B., Christiansen, A. V., & Auken, E. (2009). A review of helicopter-borne electromagnetic methods for groundwater exploration. *Near Surface Geophysics*, *7*, 629–646. https://doi.org/10.3997/1873-0604.2009043

Simmons, C. T., Fenstemaker, T. R., & Sharp, J. M. (2001). Variable-density groundwater flow and solute transport in heterogeneous porous media: Approaches, resolutions and future challenges. *Journal of Contaminant Hydrology*, *52*, 245–275. https://doi.org/10.1016/S0169-7722(01)00160-7

Sonnenborg, T. O., Scharling, P. B., Hinsby, K., Rasmussen, E. S., & Engesgaard, P. (2016). Aquifer vulnerability assessment based on sequence stratigraphic and ^{39}Ar transport modeling. *Groundwater*, *54*(2), 214–230. https://doi.org/10.1111/gwat.12345

Sørensen, K. I., & Auken, E. (2004). SkyTEM—A new high-resolution transient electromagnetic system. *Exploration Geophysics*, *35*, 191–199. https://doi.org/10.1071/EG04194

Sterckx, A., Lemieux, J. M., & Vaikmäe, R. (2017). https://doi.org/10.11 55/2017/4598902

Stroeven, A. P., Hättestrand, C., Kleman, J., Heyman, J., Fabel, D., Fredin, O., et al. (2016). Deglaciation of Fennoscandia. *Quaternary Science Reviews*, *147*, 91–121. https://doi.org/10.1016/j.quascirev.2015.09.016

Stuyfzand, P. J. (2008). Base exchange indices as indicators of salinization or freshening of (coastal) aquifers. 20th salt water intrusion meet (pp. 262–265). Naples, FL USA. Retrieved from http://www.swim-site.nl/pdf/swim20/file281-284.pdf

Sulzbacher, H., Wiederhold, H., Siemon, B., Grinat, M., Igel, J., Burschil, T., et al. (2012). Numerical modelling of climate change impacts on freshwater lenses on the North Sea Island of Borkum using hydrological and geophysical methods. *Hydrology and Earth System Sciences*, *16*, 3621–3643. https://doi.org/10.5194/hess-16-3621-2012

Van Roosmalen, L., Sonnenborg, T. O., & Jensen, K. H. (2009). Impact of climate and land use change on the hydrology of a large-scale agricultural catchment. *Water Resources Research*, *45*, W00A15. https://doi.org/10.1029/2007WR006760

Walther, M., Graf, T., Kolditz, O., Liedl, R., & Post, V. (2017). How significant is the slope of the sea-side boundary for modelling seawater intrusion in coastal aquifers. *Journal of Hydrology*, *551*, 648–659. https://doi.org/10.1016/j.jhydrol.2017.02.031

Webb, M. D., & Howard, K. W. F. (2011). Modeling the transient response of saline intrusion to rising sea-levels. *Ground Water*, *49*, 560–569. https://doi.org/10.1111/j.1745-6584.2010.00758.x

Werner, A. D., Bakker, M., Post, V. E. a., Vandenbohede, A., Lu, C., Ataie-Ashtiani, B., et al. (2013). Seawater intrusion processes, investigation and management: Recent advances and future challenges. *Advances in Water Resources*, *51*, 3–26. https://doi.org/10.1016/j.advwatres.2012.03.004

Werner, A. D., & Simmons, C. T. (2009). Impact of sea-level rise on sea water intrusion in coastal aquifers. *Ground Water*, *47*, 197–204. https://doi.org/10.1111/j.1745-6584.2008.00535.x

Winter, T. C. (1978). Numerical simulation of steady state three-dimensional groundwater flow near lakes. *Water Resources Research*, *14*(2), 245–254. https://doi.org/10.1029/WR014i002p00245